Research Article Vol. 34, No. 3 / 9 Feb 2026 / Optics Express 3732
Optics EXPRESS

# Investigating the performance of adaptive optics on different bases of spatial modes in turbulent channels

ROJAN ABOLHASSANI,[1] LUKAS SCARFE,[1,5] FRANCESCO DI COLANDREA,[1,2] ALESSIO D'ERRICO,[1,3] KHABAT HESHAMI,[1,3] AND EBRAHIM KARIMI[1,3,4,6]

[1]*Nexus for Quantum Technologies, University of Ottawa, Ottawa, K1N 6N5, ON, Canada*
[2]*Dipartimento di Fisica "Ettore Pancini", Università Degli Studi di Napoli Federico II, Complesso Universitario di Monte Sant'Angelo, Via Cintia, 80126 Napoli, Italy*
[3]*National Research Council of Canada, 100 Sussex Drive, Ottawa, K1A 0R6, ON, Canada*
[4]*Institute for Quantum Studies, Chapman University, Orange, California 92866, USA*
[5]*lscar039@uottawa.ca*
[6]*ekarimi@uottawa.ca*

**Abstract:** Quantum key distribution (QKD) allows secure key exchange based on the principles of quantum mechanics, with higher-dimensional photonic states offering enhanced channel capacity and resilience to noise. Free-space QKD is crucial for global networks where fibres are impractical, but atmospheric turbulence introduces severe states' distortions, particularly for spatial modes. Adaptive optics (AO) provides a pathway to correct these errors, though its effectiveness depends on the encoding basis. Here, we experimentally evaluate a high-speed AO system for orbital angular momentum (OAM) modes, mutually unbiased bases (MUB), and symmetric, informationally complete, positive operator-valued measures (SIC-POVM) up to dimension $d = 8$ in a turbulent free-space channel. While OAM states are strongly distorted, their cylindrical symmetry makes them optimally corrected by AO, yielding error rates below QKD security thresholds. MUB and SIC-POVM exhibit greater intrinsic robustness to turbulence but are less precisely corrected; however their performance remains within protocol tolerances. These results establish AO as a key enabler of secure, high-dimensional QKD and highlight the role of basis choice in optimizing resilience and correction.



## 1. Introduction

Quantum key distribution (QKD) is a method of sharing a secure key over a public channel, where the sender, Alice, aims to establish a shared secure key with the receiver, Bob. The two parties, along with an eavesdropper, Eve, with access to the public channel, are only limited by the laws of physics

QKD can be implemented using different protocols, all based on the same fundamental principles, where the security of the communication is ensured by the impossibility of cloning unknown quantum states with 100% fidelity [1]. These protocols mostly differ in the set of non-orthogonal bases they use. Some of the most well-known protocols include the BB84 [2], the MUB (tomographic) protocol [3], or the Singapore protocol [4] – see [5] for a comprehensive survey of various QKD protocols employing spatial modes of light. By going to higher dimensions, having access to a larger alphabet, it is possible to encode more bits per sifted photons. This suggests that higher dimensions can increase the amount of secure information density per photon [6]. Moreover, higher-dimensional QKD protocols exhibit greater resilience to noise, thereby increasing the security threshold required to obtain a positive key in the presence of potential eavesdroppers [7].

#582413 https://doi.org/10.1364/OE.582413
Journal © 2026 Received 23 Oct 2025; revised 13 Dec 2025; accepted 30 Dec 2025; published 26 Jan 2026

Optics EXPRESS

While polarization is limited to two-dimensional (qubit) information encoding, spatial modes of light can be harnessed to encode quantum information in high-dimensional spaces [8–10]. A widely used spatial mode encoding makes use of superpositions of modes carrying orbital angular momentum (OAM). We can theoretically have unbounded orthogonal OAM-carrying states, and thus, encode information in $d$-dimensions rather than only two dimensions, hence the name qu*d*its instead of qu*b*its. These OAM carrying beams have a helical phase structure $e^{i\ell\phi}$, where $\phi$ is the azimuthal angle in cylindrical coordinates and $\ell$ is the topological charge, an integer representing the number of $2\pi$ phase windings around the beam axis. In addition, proper superpositions of these modes that form a new set of orthogonal modes can also be used as new bases for information carriers in QKD protocols [11].

QKD using spatial modes of light has been demonstrated in different channels such as optical fibres, [12–14], underwater [15–17], or free space [18]. Free-space QKD can be implemented in places where fibre channels are not accessible, and is essential in scenarios such as satellite communications. One of the main obstacles faced in free-space QKD is the atmospheric turbulence, which can completely distort the phase of the signal beam, reducing or even compromising the security of the channel.

When the turbulence effects are weak enough to introduce mostly phase distortion and negligible amplitude modulations, we can compensate for the environmental noise by using fast adaptive optics (AO) systems [19,20]. The use of adaptive optics has also been demonstrated to compensate for turbulence and preserve entanglement of two photons, which can be used to implement entanglement-based QKD [21]. Since adaptive optics systems have limited spatial resolution, their performance may vary depending on the selected sets of spatial modes. Therefore, not all modes behave the same under the same circumstances.

Here, we investigate the behaviour and performance of different high-dimensional superpositions of the OAM modes in the form of mutually unbiased bases (MUB) [22] and symmetric informationally complete positive operator-valued measure (SIC-POVM) [4] in turbulent channels. Our goal is to identify the optimal modes which are less vulnerable to turbulence and more effectively corrected using AO. Our findings indicate that AO systems achieve the highest correction performance for pure OAM modes; however, these modes are also the most sensitive to turbulence. In contrast, certain MUB superpositions demonstrate greater resilience to turbulence, though their error rates remain somewhat higher than those of the OAM basis. Nevertheless, the application of AO enables recovery of channel security, balancing resilience and correctability across different mode sets.

## 2. Theory

We begin by outlining the definitions of the basis sets considered in this work. The set of modes which carry quantised non-zero orbital angular momentum, $\{|\ell\}\rangle_{\ell\neq 0}$, is considered as the *logical* basis. The position $\mathbf{r}$ representation of these modes is considered to be Laguerre-Gaussian (LG) modes, $\langle \mathbf{r}|\ell| :\rangle = \mathrm{LG}_{\ell,p=0}(\mathbf{r})$, in transverse profile [23]. Here, $p$ is the radial index, but for simplicity, we consider it to be equal to zero; apart from a normalization factor, the expression for such a beam is given by $r^{|\ell|}\, e^{i\ell\phi}\, e^{-(r/w_0)^2}$ with $w_0$ being the mode's beam waist.

### 2.1. Mutually unbiased bases

Mutually unbiased bases (MUB) are a set of bases, each consisting of an orthonormal and complete set of elements, in which each vector basis or element has the following relation with other elements from the different basis sets:

$$\left|\langle \beta_i^{(a)} | \beta_j^{(b)} \rangle\right|^2 = \frac{1}{d}, \quad a \neq b \tag{1}$$

Optics EXPRESS

where $\beta_i^{(a,b)}$ are elements of the basis $(a)$ or $(b)$, $i, j \in (1, d)$ and $d$ is the dimension of the Hilbert space. We investigate every MUB in dimensions $d = 2, 3, 4, 5, 8$, of which there are $d + 1$ MUB. In each MUB, there are $d$ orthogonal vectors. Sets of $d+1$ MUB are known to exist in dimensions which are integer powers of a prime $d = p^n$ [22,24]. Determining maximal sets of MUB in arbitrary dimensions remains an open problem [25]; even in dimension six ($6 = 2 \times 3$), which is not a prime power, a complete construction is still unknown. In the simplest case where $d = 2$, each MUB is given by the eigenvectors of the Pauli matrices. For polarization encoding, these (2+1=3) MUB correspond to horizontal and vertical polarization ($\{|H\rangle, |V\rangle\}$), diagonal and anti-diagonal ($\{|D\rangle, |A\rangle\}$), and left and right-circular polarizations ($\{|L\rangle, |R\rangle\}$). In experiments concerning the OAM of light, we use the $\mathrm{LG}_{\ell,0}$ modes as our logical bases and use them to build sets of MUB (considering $d$ is a power of a prime number). For dimension $d$, we use $\ell$ from $\{-d, -d+1, \ldots, d-1, d\}$; however, the Gaussian mode, $\ell = 0$ was excluded for even dimensions. The Gaussian mode couples very strongly into the measurement device because of our use of a SMF, leading to disproportionately high cross-talk during the final measurement when included. In odd dimensions, however, the only symmetrical choice would be to use the Gaussian mode which is between the other modes. By maintaining symmetry, we limit the beam waist of the generated mode to be, at most, the beam waist of our highest order OAM mode. When using MUB, the outcome of measurement in a basis different from the logical basis has the same probability for each input OAM value; therefore, no information about its preparation could be obtained by the eavesdropper.

### 2.2. Angular basis

In the realm of high-dimensional QKD, the most commonly utilized secondary basis is generated by applying the discrete quantum Fourier transform to the logical OAM basis:

$$|\phi_k\rangle = \frac{1}{\sqrt{d}} \sum_{j=0}^{d-1} e^{2\pi i \frac{jk}{d}} |j\rangle, \tag{2}$$

where $|j\rangle = \frac{d}{2} + (l-1)\Theta(\ell) + \ell\Theta(-\ell)$ and $\Theta$ is the Heaviside function, i.e. we use $\ell$ from $\{-d, -d+1, \ldots, d-1, d\}$ and exclude $\ell = 0$ for even dimensions. This MUB is referred to as the angular mode set when the logical basis is given by OAM eigenstates and is characterized by basis elements with peak intensity located at a specific azimuthal angle $\phi = 2\pi k/d$. This angular basis yields the same states as the first MUB in the prime dimension cases. This Fourier-conjugate basis exhibits mutual unbiasedness with respect to the logical basis, indicating that a state prepared in one basis will produce uniformly random measurement outcomes when assessed in the other. Such complementary relationships are crucial for ensuring the security of QKD protocols, as they enable the detection of potential eavesdropping through heightened error rates in the conjugate measurements.

### 2.3. SIC-POVM

Positive operator-valued measures (POVMs) are sets of positive semidefinite operators that describe generalized measurements on a quantum state. A POVM is said to be informationally complete (IC) if its measurement outcomes uniquely determine the state. Among these, a particularly important class is the symmetric informationally complete POVMs (SIC-POVMs), in which all elements share the same pairwise inner product, making them maximally efficient. Such sets provide a minimal spanning of the Bloch sphere and are widely regarded as optimal for state reconstruction [26]. It has been shown that in group-covariant cases, there are SIC-POVMs in all finite dimensions. SIC-POVMs in dimension $d$ are a set of $d^2$ normalized vectors $|\phi\rangle$ such

Optics EXPRESS

that:

$$\left|\langle\phi_i|\phi_j\rangle\right|^2 = \frac{1}{(1+d)}, \quad i \neq j\,. \tag{3}$$

Completeness and informational completeness both follow from this property. One way of creating SIC-POVM elements is by applying the operator $D_{ij}$

$$D_{ij} = \omega^{jm}|k \oplus m\rangle\langle m|, \tag{4}$$

to a Fiducial vector $|\phi\rangle$ [26]. In this case $\oplus$ is the addition modulo $d$ and $\omega = \exp(2\pi i/d)$. In dimension $d = 2$, the SIC-POVM corresponds to four pure states forming the vertices of a tetrahedron on the Bloch (Poincaré) sphere, which are mutually non-orthogonal. Such SIC-POVM bases have been employed in QKD protocols, for instance, in the Singapore protocol [4,27], which exhibits higher error tolerance compared with traditional MUB (tomographic)- and BB84-based schemes.

## 3. Experiment

### 3.1. Experimental setup

The experimental setup consists of three main components: a sender (Alice), who prepares and encodes high-dimensional quantum information onto the spatial structure of photons; a turbulent channel, implemented using a controllable hotplate inside a 30 cm-wide glass tank; and a receiver (Bob), who ultimately decodes the transmitted states. The information-carrying beam is referred to as the signal beam. Alice prepares a continuous-wave 633 nm laser and directs it onto a phase-only spatial light modulator (SLM) to encode the desired state. We use a Holoeye PLUTO/HES 6010 SLM. This SLM has a resolution of $1920 \times 1080$ pixels with a pixel pitch of 8.0 µm. By imprinting computer-generated holograms, the SLM modulates both the phase and the amplitude profile of the incoming beam [28,29], thereby creating high-dimensional spatial modes for transmission (see Fig. 1). In parallel, a second laser produces a Gaussian reference beam that is introduced into the system to probe and compensate for turbulence. This reference beam is prepared with a polarization state orthogonal to that of the signal, ensuring that the two beams can be deterministically separated at later stages of the experiment. The signal and reference beams are combined at a polarizing beam splitter (PBS) and propagate collinearly through the turbulence cell, where both experience identical wavefront distortions. The turbulence itself is generated by the convection currents of a controlled hotplate placed at the base of the glass tank, producing refractive-index fluctuations representative of atmospheric conditions. After traversing the turbulence, the composite beam is directed to the AO system which consists of a deformable mirror (DM9725, ALPAO) with a diameter of 22.5 mm, with 97 actuators divided in an $11 \times 11$ grid along with a Shack–Hartmann wavefront sensor (SH-CMOS fast, ALPAO) that has a 7.17mm diameter consisting of 64x64 subapertures, and a pitch of 112 µm. The wavefront sensor (WFS) and deformable mirror (DM) are connected in a closed-loop control configuration, allowing the DM to actively reshape its surface in response to the measured aberrations and thereby compensate for turbulence-induced distortions. Following this correction, the reference and signal beams are separated by a second PBS: the reference beam is sent to the WFS for continuous monitoring, while the signal beam is directed to Bob. At the receiver, Bob performs projective measurements on the signal beam over the chosen set of spatial modes. Here, the measurements are implemented using an intensity-flattening approach: a second SLM is programmed with phase masks that convert the incoming spatial modes into Gaussian-like profiles, which are then coupled into a SMF and detected [30]. The second SLM is a Santec SLM-100 with a resolution of $1440 \times 1050$ and a pixel pitch of 10 µm. We achieve high mode selectivity and allows faithful discrimination between the high-dimensional states transmitted through the channel. To characterize the level of turbulence introduced in the experiment, we

Optics EXPRESS

compared the measured cross-talk matrices with theoretical predictions under different turbulence strengths. Agreement between simulation and experiment allowed us to estimate the effective refractive-index structure constant, $C_n^2 \approx 10^{-14.7}$ [31], which is typical of moderate atmospheric turbulence. We maintained this turbulence strength throughout all measurements. While at any instantaneous moment the exact conditions of the turbulence could be higher or lower than our measured $C_n^2$, the average over our measurements is the relevant value. This turbulence strength was selected by increasing the temperature of the hotplate until the AO system was no longer capable of compensating for our reference Gaussian beam and then reducing the temperature slightly. Further details of the turbulence modelling and numerical simulations are provided in the Supplement 1.

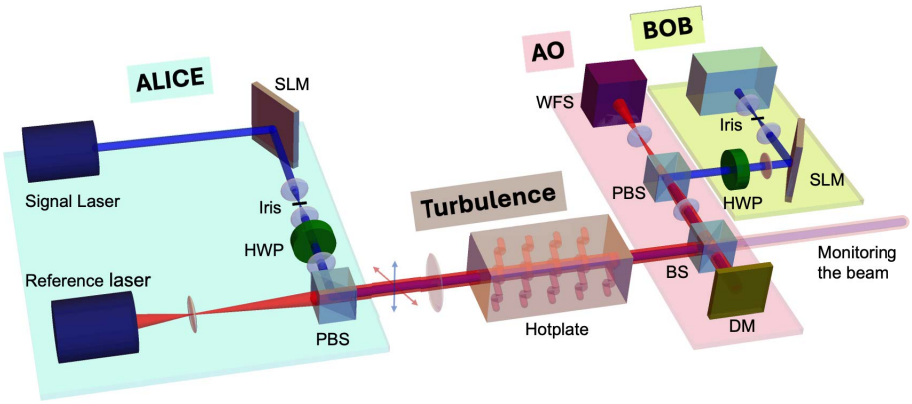


**Fig. 1.** Experimental setup for transmitting quantum states of light and testing MUB, SIC-POVM, and Angular states through turbulent media. Turbulence is generated using a controllable hotplate placed inside a 30-cm-wide glass tank. The signal beam, encoded with spatial mode information (MUB, SIC-POVM, or Angular) via a spatial light modulator (SLM), is combined with the reference beam at a polarizing beam splitter (PBS) and both co-propagate through the turbulence cell. The composite beam is then split by a 50:50 beam splitter (BS): one part is directed to a side wavefront sensor (WFS) to monitor the output wavefront, while the other part is sent to the adaptive optics (AO) system (from ALPAO). The AO system consists of a deformable mirror (DM) and a WFS operating in closed-loop feedback, where the DM corrects distortions measured by the WFS. After AO correction, the signal and reference beams are separated using a PBS. The signal component is then directed to a second SLM, which performs projective measurements of the spatial modes and couples the selected mode into a single-mode fibre (SMF) for detection, while the reference beam is sent to the WFS.

### 3.2. *Cross-talk matrix and QDER measurements*

For each incoming basis, $\{|\psi_j\rangle\}$, Bob performs projective measurements of the signal beam onto the different modes, $\{|\langle\psi_i|\}$. In the case of MUB and angular (ANG) modes, the cross-talk is quantified by evaluating the projection probabilities $|\langle\psi_i|\psi_j\rangle|^2$ across all modes within the basis. To normalize the projective measurement matrix, each row is scaled so that its sum equals one. The resulting normalized matrix defines the cross-talk distribution:

$$C_{i,j} = \frac{|\langle\psi_i|\psi_j\rangle|^2}{\Sigma_{i=0}^{d-1}|\langle\psi_i|\psi_j\rangle|^2}. \tag{5}$$

The key metric used to assess the communication performance and analyze the security is the quantum dit error rate (QDER). It is obtained by calculating the average of the diagonal elements

Optics EXPRESS

of the normalized cross-talk matrix, and subtracting this value from the theoretical maximum of unity,

$$\mathrm{QDER} = 1 - \frac{\Sigma_{i=0}^{d-1} C_{ii}}{d}. \tag{6}$$

For the SIC-POVM, the cross-talk matrix is normalized so that each row sums to $d$, i.e.,

$$C_{i,j} = d \times \frac{|\langle\psi_i|\psi_j\rangle|^2}{\Sigma_{i=0}^{d^2-1}|\langle\psi_i|\psi_j\rangle|^2}. \tag{7}$$

In analogy to the MUB-based protocols, the QDER for SIC-POVMs can be estimated from the following expression:

$$\mathrm{QDER} = 1 - \frac{\mathrm{Tr}[C_{ii}]}{d^2}. \tag{8}$$

Here, $\mathrm{Tr}(\cdot)$ denotes the trace operation, applied to the cross-talk matrix. The quantum error is then obtained by subtracting the average of the diagonal elements of the measured matrix from the corresponding theoretical value.

### 3.3. Turbulence compensation

Phase distortions induced by turbulence are corrected using a closed-loop AO system from ALPAO. The AO system comprises three primary components: a Shack–Hartmann wavefront sensor (WFS), a control computer, and a deformable mirror (DM). Unlike earlier AO systems based on segmented mirror arrays, the DM employed here consists of a continuous reflective surface actuated by 97 electromagnetic elements. This design eliminates aberrations that would otherwise arise from inter-element gaps [32]. By locally adjusting the mirror surface, the DM reshapes the reflected beam in real time. The signal and reference beams are separated at a polarizing beam splitter (PBS), with the reference beam directed to the WFS. The Shack–Hartmann WFS samples the wavefront by measuring the displacement of focal spots relative to their ideal positions on the detector array. These displacements are then decomposed into Zernike polynomials, a widely used set of orthonormal functions for describing optical aberrations [33]. Each polynomial corresponds to a distinct type of aberration (e.g., defocus, astigmatism, coma), enabling a compact representation of the measured wavefront distortion. This wavefront information is processed by the control computer, which generates the corresponding corrective commands for the DM. By applying the conjugate phase to the incoming distorted beam, the DM compensates for the turbulence-induced aberrations. The feedback loop operates at kilohertz rates: the WFS used here functions at 1 kHz (with a maximum capability of 5 kHz), while the turbulence dynamics are on the order of 100 Hz. Thus, the AO corrections are effectively applied in real time relative to the evolution of the turbulent channel.

### 3.4. Experimental results

Using the setup described above, we performed experiments across different QKD protocols and Hilbert-space dimensions, evaluating the effects of turbulence and the corrective performance of the AO system. For each dimension, we measured the cross-talk matrices and extracted the corresponding QDER, both with AO disabled and enabled. Figure 2 shows the measured cross-talk matrices for different dimensions under both conditions, alongside numerical simulations based on the expected turbulence strength. From these results, QDER values were calculated for each basis and dimension. The corresponding results are summarized in Fig. 3, which presents the QDER for MUB, OAM modes, and ANG modes in dimensions $d = 2, 3, 4, 5, 6$, and 8. We note that in the case of $d = 6$, which is not a prime power, only three MUB are known [34,35]; the analysis is therefore restricted to OAM and ANG modes, with the SIC-POVM case discussed separately.

Optics EXPRESS

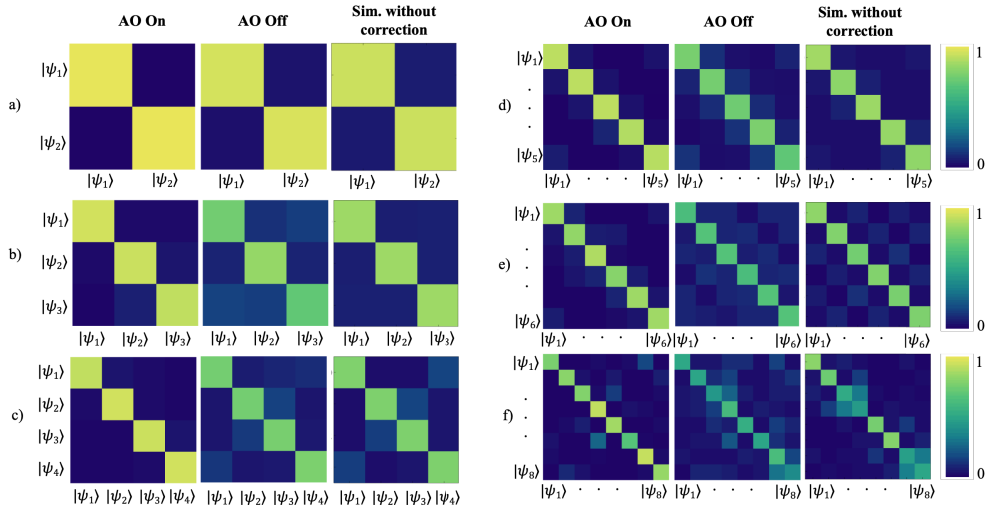


**Fig. 2.** Cross-talk matrices of the first MUB for dimensions a) $d = 2$, b) $d = 3$, c) $d = 4$, d) $d = 5$, e) $d = 6$, and f) $d = 8$. Each panel displays three matrices for comparison: the first shows the experimental results obtained under turbulence with AO enabled (AO On), the second shows the corresponding experimental results under turbulence with AO disabled (AO Off), and the third presents numerical simulations of turbulence without correction (Sim). The comparison highlights the strong impact of turbulence on high-dimensional states and the significant improvement in mode fidelity achieved by AO correction, in close agreement with the simulated predictions.

Several clear trends emerge. First, higher-dimensional states are generally more susceptible to turbulence-induced errors. Second, activating the AO system significantly improves performance, reducing QDER values across all bases and dimensions. The AO correction is particularly effective for OAM modes, which, despite being highly distorted by turbulence, benefit strongly from the circular symmetry of the deformable mirror corrections. By contrast, certain MUB superpositions, while less corrected by AO, exhibit intrinsic robustness to turbulence due to their reduced spatial extent. These observations highlight an interplay between the geometric structure of the spatial modes and the corrective fidelity of the AO system. Modes with circularly symmetric profiles are more prone to turbulence but also more accurately corrected, whereas modes with localized lobes are less affected by turbulence but more challenging to correct. Intensity and phase profiles of these modes are shown in the Supplement 1.

The results further demonstrate that AO reduces the QDER most effectively in lower dimensions, bringing values well below the security thresholds for QKD protocols such as BB84 (two MUB) and six-state (tomographic) schemes (three MUB) [5]. Specifically, in dimension two (Fig. 3(a)), the OAM and MUB states yield comparable QDERs; the ANG or first MUB basis emerges as the optimal choice in this regime. In dimension three (Fig. 3(b)), which includes the Gaussian $\ell = 0$ mode, we observe increased cross-talk, but the first MUB still performs better under turbulence and AO correction, making it a strong candidate alongside the OAM basis. In dimension four (Fig. 3(c)), the Gaussian mode was excluded, the first MUB again shows superior resilience, while the fourth MUB is the most fragile, though still recoverable with AO. For dimension five (Fig. 3(d)), the Gaussian mode component introduces additional noise, and although all bases are impacted, only the OAM and first MUB are well corrected. In dimension six (Fig. 3(e)), where only three MUB sets are known, results are only reported for OAM and ANG modes. Finally, in dimension eight (Fig. 3(f)), even with AO, some bases yield QDER approaching the security threshold, though OAM, ANG, and the first two MUB remain viable candidates. Taken

Optics EXPRESS

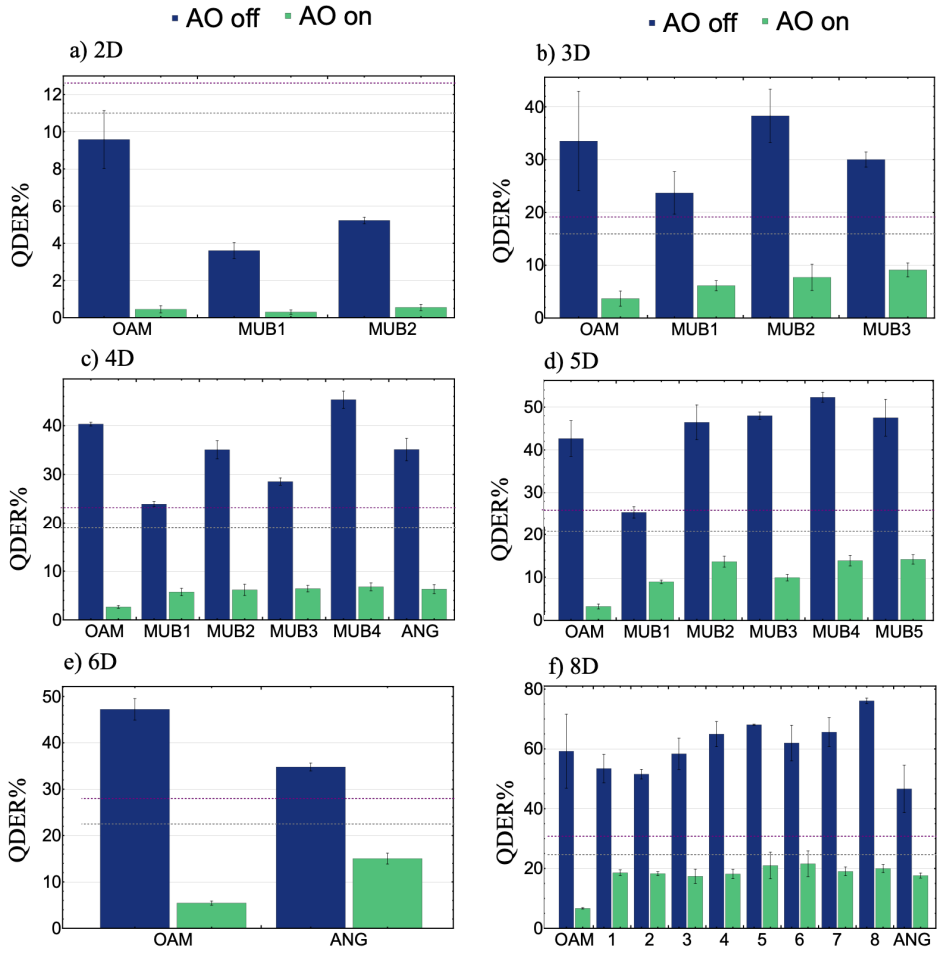


**Fig. 3.** Quantum dit error rate (QDER) measured for different basis sets and Hilbert-space dimensions under turbulent conditions, with AO On (green) and with AO Off (blue). Panels a-f correspond to dimensions 2, 3, 4, 5, 6, and 8, respectively. Each bar shows the average QDER for OAM, MUB, and ANG bases (where applicable), with error bars representing statistical uncertainties. The dotted lines show the QDER thresholds for the BB84 (gray) and six-state (purple) protocols. The error lines on the bars indicate the standard deviation of the diagonal elements of each crosstalk matrix. The results demonstrate the strong effect of turbulence on high-dimensional states and the significant reduction in QDER achieved by AO correction.

together, these results show that while turbulence strongly limits the fidelity of high-dimensional QKD, AO can substantially suppress the induced errors, bringing QDER values below security thresholds across a wide range of protocols and dimensions. This confirms the feasibility of secure, high-dimensional QKD over turbulent free-space channels when combined with an AO system. When using OAM for free-space optical experiments, several factors, e.g. numerical aperture of the entire optical system, must be considered and balanced. In our case, with our selected experimental parameters, the QDER in eight dimensions is very close to the security threshold. The next dimension with a complete set of known MUB is dimension nine. Given that it is an odd dimension, the Gaussian mode will cause excess noise and will thus surpass the security threshold. Furthermore, by going to higher OAM-based dimensions, the size of the

Optics EXPRESS

beam increases, which limits the use of our AO system. We could then reduce the size of the beam using other experimental means, which would increase the error rate of the lower-valued OAM modes and also cause larger beam divergence.

Beyond testing the maximal sets of MUB available in a given dimension $d$, it is also important to evaluate the capability of our AO system with other classes of states, thereby demonstrating its versatility for a broader range of quantum communication protocols. In particular, since no complete set of MUB exists in dimension six, we consider alternative measurement frameworks such as SIC-POVMs, which in bi-dimensional space form the basis of the Singapore protocol [4]. Our experimental results (Fig. 4) show that SIC-POVM states are strongly affected by turbulence, leading to substantial cross-talk and elevated QDER. However, when AO correction is applied, the QDER is significantly reduced across all tested dimensions ($d = 2, 3, 4$, and 6), with values falling below the theoretical security threshold of the Singapore protocol. This demonstrates that while SIC-POVMs are inherently fragile in turbulent environments, AO correction restores their viability for secure quantum key distribution. The cross-talk matrices further confirm this conclusion: with AO enabled, the measured mode overlaps approach the expected theoretical distributions, in close agreement with numerical simulations. These results highlight both the susceptibility of SIC-POVM states to channel-induced distortions and the ability of AO systems to extend their practical utility in high-dimensional quantum communication protocols.

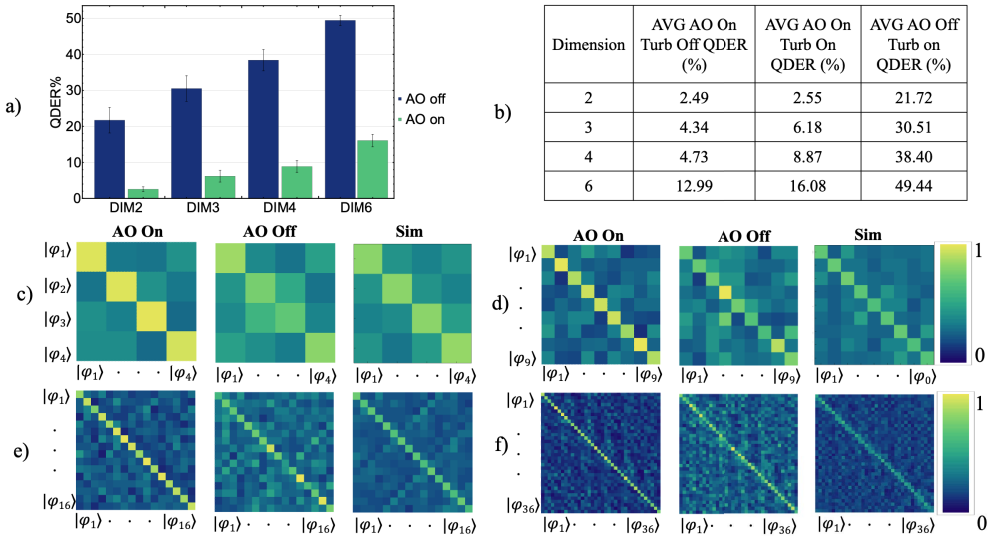


| Dimension | AVG AO On Turb Off QDER (%) | AVG AO On Turb On QDER (%) | AVG AO Off Turb on QDER (%) |
|---|---|---|---|
| 2 | 2.49 | 2.55 | 21.72 |
| 3 | 4.34 | 6.18 | 30.51 |
| 4 | 4.73 | 8.87 | 38.40 |
| 6 | 12.99 | 16.08 | 49.44 |

**Fig. 4.** Cross-talk matrices and QDER for SIC-POVM modes under turbulence with and without AO correction. (a) Measured QDER for SIC-POVM modes transmitted through a turbulent channel, comparing AO-enabled (green) and AO-disabled (blue) scenarios. (b) Table summarizing the average QDER values obtained experimentally for SIC-POVM states in dimensions $d = 2$, $d = 3$, $d = 4$, and $d = 6$ under different conditions. (c–f) Experimental cross-talk matrices for SIC-POVM modes in dimensions 2, 3, 4, and 6, respectively, shown for AO enabled (AO On), AO disabled (AO Off), and numerical simulations of turbulence without correction (Sim). These results demonstrate the vulnerability of SIC-POVM states to turbulence and the significant reduction in error achieved by AO correction.

The security thresholds for different protocols are summarized in Table S1. of the Supplement 1 for comparison [5]. Our results demonstrate that with AO correction, QKD can be implemented in turbulent channels while keeping error rates below the relevant security thresholds. At the same time, the results reveal that the AO system is not universal: it provides the most effective

Optics EXPRESS

correction for specific mode families, particularly OAM modes. We also observe that certain modes exhibit greater intrinsic robustness to turbulence owing to their spatial localization.

## 4. Conclusion

In summary, we have systematically investigated the behaviour of all known MUB and SIC-POVMs in multiple dimensions, up to $d = 8$, under turbulence, and assessed the effectiveness of their correction using AO. These results provide practical guidance for selecting the most suitable basis sets under different channel conditions and for different QKD protocols. In particular, we find that in low-turbulence regimes, the OAM basis–although most strongly distorted by turbulence–benefits most from AO correction and thus emerges as the optimal channel for information transmission. This suggests that when using AO, QKD schemes could be implemented such that the logical (OAM) basis, which has a lower error rate, can be used most of the time while the MUB with a higher error rate is employed less often, primarily for security checks, thus leveraging an unbalanced usage of the bases [36]. This technique of efficient encoding is known to allow for more bits of information to be used for key generation when errors are more pronounced in a particular basis. While our work focuses on scalar modes of light, the same techniques could be applied to vector modes for optimal determination of modes in different conditions. Indeed, one could implement so-called "vectorial adaptive optics (V-AO)" [37] to further improve results in such a basis. We also plan to test the present setup with vector modes. The DM is metallic, thus it should apply the same phase shift to both polarization components. If turbulence is optically anisotropic, the adaptive optics should correct for both polarization channels. We also plan to test the present setup with vector modes. The DM is metallic, thus should apply the same phase shift to both polarization components. If turbulence is optically anisotropic, the adaptive optics should correct for both polarization channels. Beyond QKD, the implications of our results extend to other domains that rely on spatial modes of light. In biological imaging and microscopy, where turbulence and aberrations are often unavoidable, AO can mitigate distortions when using Fourier conjugates of OAM modes [38–40]. Similarly, our findings indicate that AO correction can enhance the performance of vortex-beam-based coronagraphy [41–43], further underscoring the broad applicability of these techniques.

**Funding.** PNRR MUR (E0000023-NQSTI); Canada Research Chairs; National Research Council Canada (HTSN Challenge Program); Qeyssat User INvestigation Team (QUINT) Alliance Consortia; Alliance for Research and Applications of Quantum Network Entanglement (ARAQNE) Alliance Consortia.

**Disclosures.** The authors declare no conflicts of interest.

**Data availability.** Data underlying the results presented in this paper are not publicly available at this time but may be obtained from the authors upon reasonable request.

**Supplemental document.** See Supplement 1 for supporting content.

## References

1. W. K. Wootters and W. H. Zurek, "A single quantum cannot be cloned," Nature **299**(5886), 802–803 (1982).
2. C. H. Bennett and G. Brassard, "Quantum cryptography: Public key distribution and coin tossing," in *Proceedings of the IEEE International Conference on Computers, Systems, and Signal Processing*, (IEEE, Bangalore, India, 1984), pp. 175–179.
3. D. Bruß, "Optimal eavesdropping in quantum cryptography with six states," Phys. Rev. Lett. **81**(14), 3018–3021 (1998).
4. B.-G. Englert, C. Kurtsiefer, K. W. Moh, *et al.*, "Efficient and robust quantum key distribution with minimal state tomography," arXiv (2004).
5. F. Bouchard, K. Heshami, D. G. England, *et al.*, "Experimental investigation of quantum key distribution protocols with twisted photons," Quantum **2**, 111 (2018).
6. N. J. Cerf, M. Bourennane, A. Karlsson, *et al.*, "Security of quantum key distribution using *d*-level systems," Phys. Rev. Lett. **88**(12), 127902 (2002).
7. S. Ecker, F. Bouchard, L. Bulla, *et al.*, "Overcoming noise in entanglement distribution," PRX Quantum **4**, 010304 (2023).

Optics EXPRESS


8. G. Molina-Terriza, J. P. Torres, and L. Torner, "Management of the angular momentum of light: Preparation of photons in multidimensional vector states of angular momentum," Phys. Rev. Lett. **88**(1), 013601 (2001).
9. A. Mair, A. Vaziri, G. Weihs, *et al.*, "Entanglement of the orbital angular momentum states of photons," Nature **412**(6844), 313–316 (2001).
10. G. Molina-Terriza, A. Vaziri, J. Reháček, *et al.*, "Triggered qutrits for quantum communication protocols," Phys. Rev. Lett. **92**(16), 167903 (2004).
11. M. Mirhosseini, O. S. Maga na-Loaiza, M. N. O'Sullivan, *et al.*, "High-dimensional quantum cryptography with twisted light," New J. Phys. **17**(3), 033033 (2015).
12. A. Sit, R. Fickler, F. Alsaiari, *et al.*, "Quantum cryptography with structured photons through a vortex fiber," Opt. Lett. **43**(17), 4108–4111 (2018).
13. D. Cozzolino, B. Da Lio, D. Bacco, *et al.*, "Orbital angular momentum states enabling fiber-based high-dimensional quantum communication," Phys. Rev. Appl. **11**(6), 064058 (2019).
14. Q.-K. Wang, F.-X. Wang, J. Liu, *et al.*, "High-dimensional quantum cryptography with hybrid orbital-angular-momentum states through 25 km of ring-core fiber: A proof-of-concept demonstration," Phys. Rev. Appl. **15**(6), 064034 (2021).
15. A. Sit, F. Bouchard, R. Fickler, *et al.*, "High-dimensional intracity quantum cryptography with structured photons," Optica **4**(9), 1006–1010 (2017).
16. F. Bouchard, A. Sit, F. Hufnage, *et al.*, "Quantum cryptography with twisted photons through an outdoor underwater channel," Opt. Express **26**(17), 22563–22573 (2018).
17. F. Hufnagel, Y. D. Kim, H. W. Lee, *et al.*, "Characterization of an underwater channel for quantum communications in the ottawa river," Opt. Express **27**(19), 26346–26354 (2019).
18. G. Gibson, J. Courtial, M. J. Padgett, *et al.*, "Free-space information transfer using light beams carrying orbital angular momentum," Opt. Express **12**(22), 5448–5456 (2004).
19. L. Scarfe, F. Hufnagel, M. F. Ferrer-Garcia, *et al.*, "Fast adaptive optics for high-dimensional quantum communications in turbulent channels," Commun. Phys. **8**(1), 79 (2025).
20. J. Zhao, Y. Zhou, B. Braverman, *et al.*, "Real-time adaptive optics compensation in a turbulent channel with high-dimensional spatial-mode encoding," Opt. Express **28**(10), 15376–15391 (2020).
21. N. Leonhard, G. Sorelli, V. N. Shatokhin, *et al.*, "Protecting entanglement of twisted photons by adaptive optics," Phys. Rev. A **97**(1), 012321 (2018).
22. T. Durt, B.-G. Englert, I. Bengtsson, *et al.*, "On mutually unbiased bases," Int. J. Quantum Inform. **08**(04), 535–640 (2010).
23. L. Allen, M. W. Beijersbergen, R. J. C. Spreeuw, *et al.*, "Orbital angular momentum of light and the transformation of laguerre-gaussian laser modes," Phys. Rev. A **45**(11), 8185–8189 (1992).
24. W. K. Wootters and B. D. Fields, "Optimal state-determination by mutually unbiased measurements," Ann. Phys. **191**(2), 363–381 (1989).
25. P. Raynal, X. Lü, and B.-G. Englert, "Mutually unbiased bases in six dimensions: The four most distant bases," Phys. Rev. A **83**(6), 062303 (2011).
26. J. M. Renes, R. Blume-Kohout, A. J. Scott, *et al.*, "Symmetric informationally complete quantum measurements," J. Math. Phys. **45**(6), 2171–2180 (2004).
27. M. Rambach, M. Qaryan, M. Kewming, *et al.*, "Robust and efficient high-dimensional quantum state tomography," Phys. Rev. Lett. **126**(10), 100402 (2021).
28. E. Bolduc, N. Bent, E. Santamato, *et al.*, "Exact solution to simultaneous intensity and phase encryption with a single phase-only hologram," Opt. Lett. **38**(18), 3546–3549 (2013).
29. J. P. Kirk and A. L. Jones, "Phase-only complex-valued spatial filter," J. Opt. Soc. Am. **61**(8), 1023–1028 (1971).
30. F. Bouchard, N. H. Valencia, F. Brandt, *et al.*, "Measuring azimuthal and radial modes of photons," Opt. Express **26**(24), 31925–31941 (2018).
31. V. I. Tatarski, *Wave propagation in a turbulent medium* (Courier Dover Publications, 2016).
32. R. K. Tyson, *Principles of Adaptive Optics* (CRC Press, Boca Raton, 2015), 4th ed.
33. A. J. E. M. Janssen, "Zernike expansion of derivatives and laplacians of the zernike circle polynomials," J. Opt. Soc. Am. A **31**(7), 1604–1613 (2014).
34. S. Brierley and S. Weigert, "Maximal sets of mutually unbiased quantum states in dimension 6," Phys. Rev. A **78**(4), 042312 (2008).
35. S. Brierley and S. Weigert, "Constructing mutually unbiased bases in dimension six," Phys. Rev. A **79**(5), 052316 (2009).
36. H.-K. Lo, H. F. Chau, and M. Ardehali, "Efficient quantum key distribution scheme and a proof of its unconditional security," J. Cryptology **18**(2), 133–165 (2005).
37. C. He, J. Antonello, and M. J. Booth, "Vectorial adaptive optics," eLight **3**(1), 23 (2023).
38. Z. Wu, Q. Liu, Y. Zhang, *et al.*, "Quantum-enhanced optical microscopy for subnanometer resolution imaging of protein complexes," Light: Sci. Appl. **14**(1), 97 (2025).
39. L. Li, X. Liang, W. Qin, *et al.*, "Double spiral resonant mems scanning for ultra-high-speed miniaturized optical microscopy," Optica **10**(9), 1195–1202 (2023).
40. A. A. Pushkina, G. Maltese, J. I. Costa-Filho, *et al.*, "Superresolution linear optical imaging in the far field," Phys. Rev. Lett. **127**(25), 253602 (2021).

Optics EXPRESS

41. G. Foo, D. M. Palacios, and G. A. Swartzlander, "Optical vortex coronagraph," Opt. Lett. **30**(24), 3308–3310 (2005).
42. D. M. Palacios and S. L. Hunyadi, "Low-order aberration sensitivity of an optical vortex coronagraph," Opt. Lett. **31**(20), 2981–2983 (2006).
43. D. Mawet, P. Riaud, O. Absil, *et al.*, "Annular groove phase mask coronagraph," The Astrophys. J. **633**(2), 1191–1200 (2005).